Appl. Phys. B 67, 115–123 (1998)

Applied Physics B
Lasers
and Optics

Optical and microscopy investigations of soot structure alterations by laser-induced incandescence

R.L. Vander Wal[1,*], T.M. Ticich[2], A.B. Stephens[2]

[1] NCMR@NASA-Lewis Research Center, M.S. 110-3, 21 000 Brookpark Rd., Cleveland, OH 44135, USA
(E-mail: randy@rvander.lerc.nasa.gov)
[2] Department of Chemistry, Centenary College of Louisiana, 2911 Centenary Blvd., Shreveport, LA 71134, USA
(E-mail: tticich@centenary.edu)

Received: 20 October 1997/Revised version: 16 February 1998

Abstract. Understanding the physical process of LII is central to practical implementation and accurate theoretical modelling of LII. The LII dependence upon laser fluence is shown to depend upon detection conditions thereby not providing direct information about the soot temperature or structural changes. Transmission electron microscopy, used to investigate the morphological changes induced in the soot at different laser fluences, shows increasing graphitization of the soot with increasing laser fluence. For laser fluences above $0.45 \pm 0.05\,\mathrm{J/cm^2}$ at 1064 nm, vaporization/fragmentation of soot primary particles and aggregates occurs. Optical measurements are performed using a second laser pulse to probe the effects of these changes upon the LII signal. With the exception of very low fluences, the structural changes induced in the soot lead to a decreased LII intensity produced by the second laser pulse. These two-pulse experiments also show that these changes do not alter the LII signal on timescales less than 1 μs for fluences below the vaporization threshold.

PACS: 42.62 Hk; 78.20.Dj; 82.40.Py

Laser-induced incandescence (LII) has proven to be an accurate and versatile method for the measurement of the soot volume fraction, f_v. The technique, in which a pulsed laser heats soot to incandescence, offers rapid determination of f_v with high spatial and temporal resolution. LII has been successfully applied to laminar [1–11], flickering [6–8], and turbulent [3, 5, 12, 13] gas-jet diffusion flames, as well as to premixed flames [1, 14] and systems involving heterogenous combustion [5, 15]. Despite the success and widespread use of the technique, however, there remain aspects of the LII process that are not yet well understood.

Current theoretical models of LII are based on a time-dependent energy conservation equation which includes the heat source provided by the pulsed laser light and the cooling processes of radiation, conduction and vaporization [16–20]. Mass loss through vaporization of surface material dominates cooling at high laser fluences. These heat transfer processes depend on the physical properties of soot at elevated temperatures. However, the models use values of heat capacity, emissivity, and heat of vaporization for amorphous carbon at room temperature. Additionally, these models implicitly assume that no physical changes (other than surface vaporization) occur in the soot under pulsed high-intensity laser light.

The validity of these assumptions is questionable in light of several recent experimental observations. One study found that the relative intensities of the incandescence do not scale with detected wavelength as predicted by theory [21]. Transmission electron microscopy (TEM) micrographs of laser-heated soot show structural changes induced in the soot at fluences below the vaporization threshold [22]. These changes resemble the annealing process observed in heat-treatment studies of carbon black [23]. Finally, despite thermodynamic equilibrium predictions that C_3 is the major species produced in the vaporization of carbon [24], only the production of C_2 has been observed [25].

Applications of LII that rely on theoretical modelling of the signal for interpretation, such as primary particle size measurements [19–21], mandate an accurate representation of the LII process. The accuracy of theoretical models may be of less concern when utilizing LII for f_v determination. The LII intensity in diffusion and premixed flames shows excellent correlation with f_v determined through extinction [1, 2, 5–8, 14, 15] and gravimetric sampling measurements [12]. Nevertheless, an improved understanding of the physical processes that influence the observed incandescence would facilitate the application of LII to new systems.

Central to an improved understanding of the LII process is the effect of the high-intensity laser pulse upon the soot. Few experimental measurements have clearly explored this effect [22, 26]. The dependence of the integrated LII signal upon excitation laser fluence provides limited insight. Very different fluence-dependence curves have been found which either exhibit a well-defined maximum [1, 5, 11] or a continuous increase [8] in LII signal with increasing laser fluence. The differences between such curves may reflect different experimental conditions more than changes in the soot particle

* Corresponding author

temperature. Thus, the laser fluence curves provide indirect information at best on the physical process of LII.

The LII signal exhibits changes in peak intensity and temporal evolution as the laser fluence is varied. Together with the laser fluence curves for the integrated signal, this observation suggests that the laser may bring about structural/morphological changes in the soot in addition to changing its temperature.

To directly explore the effects of laser light on soot we have designed and performed a series of optical and microscopy experiments. These experiments include (1) an investigation of the influence of detection gate width and delay upon fluence dependence curves, (2) analysis of laser-heated soot at various fluences by TEM, and (3) various two-pulse LII experiments that allow the direct observation of changes in the LII signal in real time. These experiments were designed to address the following questions:

1. What physical/structural changes occur in the soot as a function of excitation laser fluence?
2. What is the effect of these changes upon the LII signal?
3. When do these changes occur after the excitation laser pulse? This consideration could apply to a LII signal produced by a single laser pulse or by a second laser pulse that heats soot heated by a prior laser pulse.
4. How robust is LII for f_v determination at different laser fluences?

1 Experimental approach

For the dual-pulse experiments, light at 1064 nm from two identical, pulsed Nd:YAG lasers was combined by using a half-wave plate and a polarizing beamsplitter as shown in the experimental schematic in Fig. 1. A beam expansion telescope, created by combining a −50-mm focal length plano-concave and +300-mm focal length plano-convex lens, followed by a spherical cylindrical lens of 1500 mm focal length formed the laser beam into a sheet. The beam focus was placed at the center of the burner with the sheet possessing a 450-μm width at the beam focus as determined through knife-edge profiling of the beam. The energies of the two laser pulses were controlled independently by varying the flashlamp energy of each laser. Digital delay generators controlled the firing of both lasers and served to synchronize the laser pulses. The LII signal was collected using a 1 : 2 magnification telescope consisting of 50-mm-diameter 100- and 200-mm focal length plano-convex fused silica lenses. This telescope coupled the LII signal into a fused silica optical fiber which terminated at the entrance of a 0.25 m monochromator fitted with a photomultiplier tube (PMT). The 1-mm-diameter optical fiber image at the burner centerline combined with the laser sheet thickness defined the spatial resolution of the technique. The LII signal was collected with a 12-nm spectral bandwidth. A digital oscilloscope served to display the PMT signal collected from the LII and to perform data averaging by coaveraging a series of time-resolved LII signals.

The ethylene gas-jet diffusion flame used in this study was stabilized on a 11-mm I.D. nozzle surrounded by an air coflow through a 101-mm-diameter honeycomb. A chimney with windows for optical access served to stabilize the flame and provide shielding from room drafts. The fuel flow rate was 0.231 slm while the air coflow was 42.8 slm.

Thermophoretic sampling measurements were performed using a double-action air-driven piston. The dwell time of the probe within the flame was controlled by custom electronics which actuated a dual-valve solenoid to govern the pressuring air-flow. TEM grids were attached to the probe by a sandwich grid holder consisting of a 0.003-inch-thick, brass shim with a 2-mm-diameter hole exposing both sides of the TEM grid. This grid holder was attached to the insertion rod of the probe

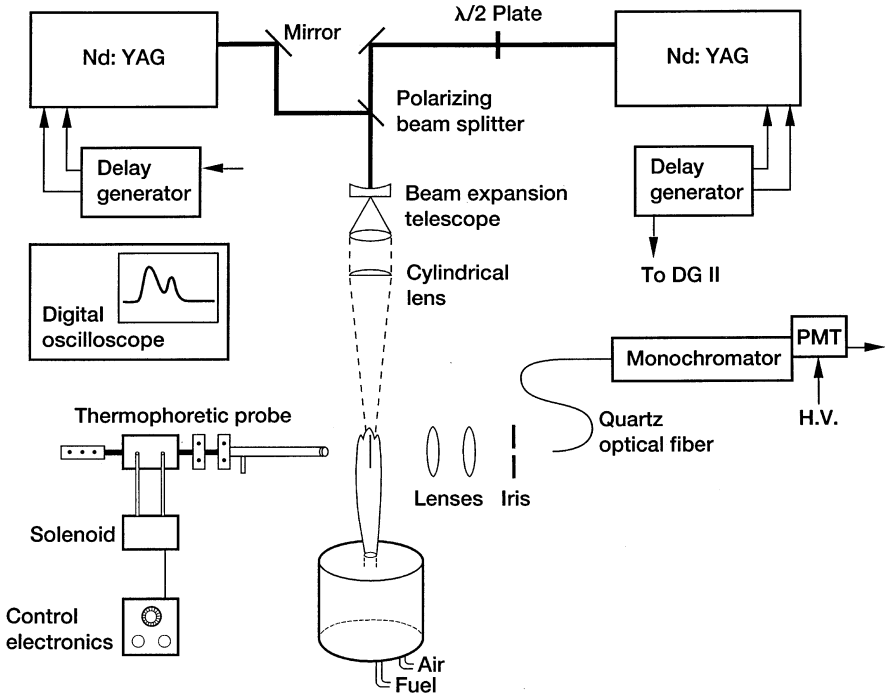

Fig. 1. Experimental schematic

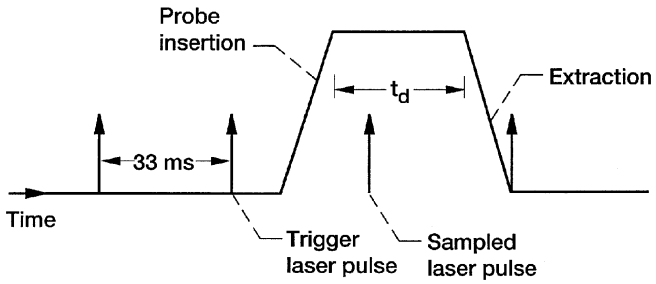

Fig. 2. Timing schematic for thermophoretic sampling probe

by a small setscrew. Further details have been published elsewhere [22]. Scattered light generated by the probe passing through a HeNe laser beam provided a temporal marker of the probe motion. In this manner the insertion, dwell, and retraction processes were characterized. Results were well represented by a trapezoid function with 10-ms insertion and retraction times as illustrated in Fig. 2. The dwell time, t_d, was variable by means of the electronics. To synchronize the probe insertion relative to the excitation laser pulse, the preceding laser pulse triggered a digital delay generator, which in turn triggered the probe insertion after an empirically determined time delay. This accounted for the mechanical delay of the probe insertion as illustrated in Fig. 2. In these experiments, the laser beam was apertured using a galvanized steel disk and left unfocussed to produce a 6-mm diameter beam with a uniform-intensity profile. The laser beam was directed through the ethylene flame at 50-mm HAB while the probe sampled the soot at a downstream position of 60-mm height above the burner (HAB). Published flow velocities [27] confirmed that a 30-ms probe residence time within the flame is sufficient to capture soot that had been heated by the laser pulse using our apparatus and timing scheme.

2 Results and discussion

2.1 Fluence dependence of LII

Figure 3 shows a fluence-dependence curve for the integrated LII signal similar to that reported elsewhere [2, 5, 11, 26]. Here, the LII intensity increases rapidly with excitation laser fluence at low fluences, reaches a plateau region for fluences between 0.4 and 0.7 J/cm^2 and then decreases at fluences greater than 0.8 J/cm^2. The rapid initial increase in the integrated signal intensity with increasing laser fluence is readily attributed to the increased emission from soot heated to higher temperatures. The plateau region can be ascribed to the soot having reached the vaporization temperature of carbon so that increased laser fluence ceases to cause substantial increases in the soot temperature. At yet higher laser fluences, laser-induced mass loss through vaporization results in less incandescing material with a concurrent signal decrease. Thus, the plateau region is thought to define a range of laser fluences that minimize signal variations induced by small fluctuations in laser intensity. LII measurements have been typically carried out in this region to maximize the signal while avoiding the difficulty of normalizing the signal. Despite its importance and utility, the fluence-dependence curve

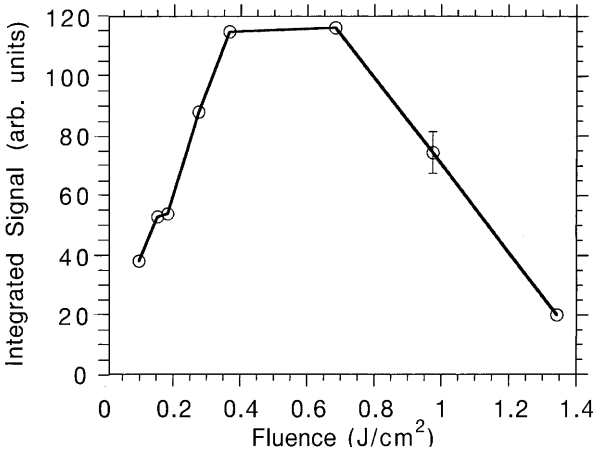

Fig. 3. Dependence of the LII intensity upon excitation laser fluence using a 50-ns-duration detection gate beginning at the peak of the LII signal

in Fig. 3 reflects one choice of experimental detection conditions (detection gate width, time delay after the laser pulse, and detection wavelength) in addition to changes in the soot by the laser. Given this, no special emphasis should be placed on using it for interpretation of the physical process of LII.

Figure 4 shows the fluence-dependence curves obtained using (a) a delayed signal collection gate, starting 100 ns after peak LII intensity with a 50 ns duration and (b) a prompt (beginning at peak LII intensity) signal collection gate, 500 ns in duration. In contrast to the fluence-dependence curve shown

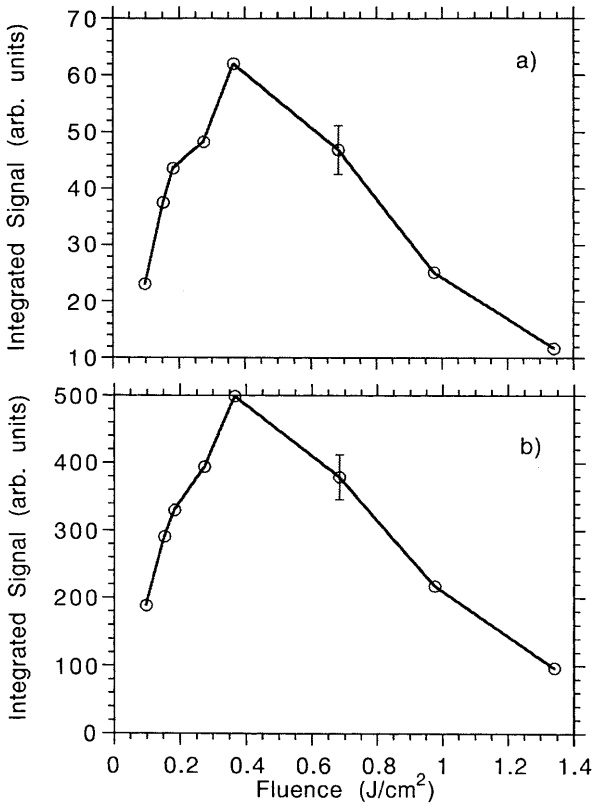

Fig. 4a,b. Dependence of the LII intensity upon excitation laser fluence using **a** a 50-ns-duration detection gate delayed from the peak intensity by 100 ns and **b** a prompt detection gate integrating the LII signal over 500 ns

in Fig. 3, which uses a prompt, 50-ns duration signal collection gate, the curves in Fig. 4 exhibit no plateau region. These results stem from the fact that both the signal intensity and temporal evolution change with laser fluence. With increasing laser fluence, there is a range of fluences for which the peak LII intensity increases while the temporal decay rate also increases. The observation of a plateau region merely reflects a trade-off between these quantities over the gate delay and duration used to integrate the LII signal. The integrated LII signal can still be converted to f_v independent of choice of conditions, provided that it is calibrated for the specific detection conditions. However, the dependence of the fluence curve on detection parameters must be explored before using the data to infer details about the laser interaction with the soot.

2.2 TEM micrographs

To address what structural/morphological changes are induced in the soot at different laser fluences, we performed TEM investigations of soot captured in situ subsequent to laser heating. Figure 5 shows soot collected from the flame after irradiation at different laser fluences and for reference,

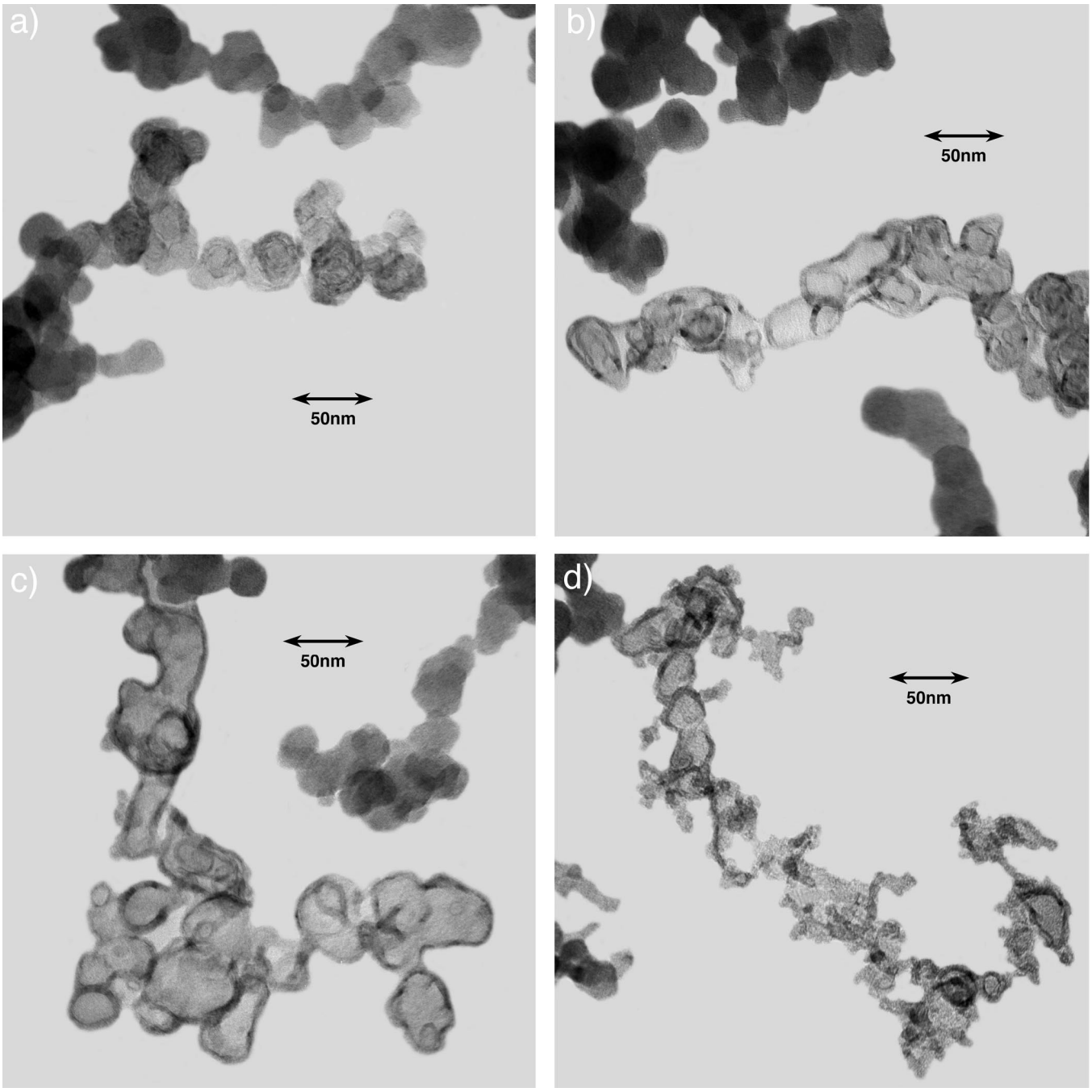

Fig. 5a–d. TEM micrographs of laser-heated soot captured via thermophoretic sampling. Values of the laser fluence were **a** 0.15, **b** 0.3, **c** 0.6, and **d** 0.9 J/cm^2

soot not subjected to laser-heating. Figure 5a shows a distinct mottled structure in portions of the micrograph, similar to a multifaceted rosette structure, for an excitation laser fluence of 0.15 J/cm^2. At a higher laser fluence of 0.3 J/cm^2 (Fig. 5b), the amount of internal material appears less. A ribbon or banded strip is observed within and around the particle perimeter for some structures. At fluences of 0.6 J/cm^2 (Fig. 5c), essentially no faceted structure can be seen within the particles whereas the ribbon structure is very pronounced both within and around the perimeter of the primary particles. Some of the structures appear to be far larger than an isolated individual primary particle, an observation significant to primary particle size determination. At these fluences, evidence of fragmentation was also observed though not as clearly as at higher fluences. At the highest fluence studied, 0.9 J/cm^2, the micrograph suggests that the shells have fragmented and that significant mass loss has occurred through laser-induced vaporization (Fig. 5d).

Figure 6 shows a high-resolution TEM micrograph of laser-heated soot using a fluence of roughly 0.4 J/cm^2. The banded or ribbon structure observed in the lower magnification images is now resolved, appearing as a series of lines. Each line corresponds to a carbon atom layer plane oriented perpendicular to the image plane. The atom planes appear dark because they block the transmission of the incident electron beam. These graphitic layer planes run parallel to each other over lengths of several nm. Angle tilting observations show these structures to be three-dimensional and hollow.

Because the basic steps of fuel pyrolysis, PAH formation/growth, and soot inception are considered to apply to soot production in general, studies of carbon black, a type of soot, are relevant to understanding soot physical structure. Heat-treatment studies of carbon black reveal structures similar to those presented in Fig. 5 and thus provide insight into our current observations [28]. X-ray diffraction studies of carbon black reveal soot particles that consist of numerous crystal-

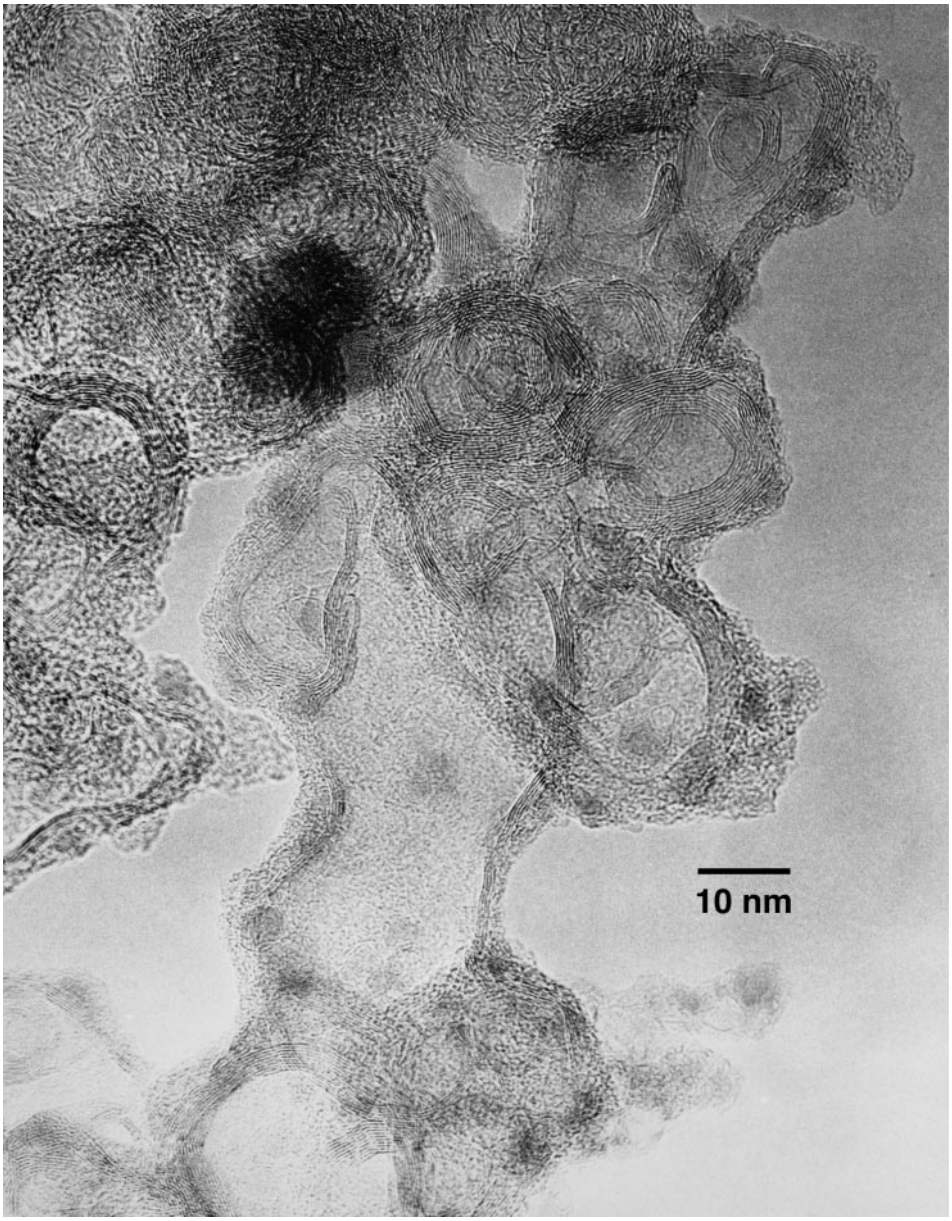

Fig. 6. High-resolution TEM micrograph of laser-heated soot

lites, on the order of 10^4 [29]. Each crystallite consists of a series of stacked carbon atom layer planes each possessing a length or breadth of several Å. With increasing elevated temperature, layer plane defects and reactive radical sites are thermally annealed [30]. Crystallite layer plane growth can occur through bonding with noncarbonaceous material within the particle. Crystallite in-plane and out-of-plane dimensions can also grow by realignment and bonding with other crystallites. With graphite being the most energetically stable form of carbon, a graphitic layer plane first forms around the particle perimeter since this surface will cool first. As cooling proceeds radially inward, this outer layer plane acts as a template for subsequent graphitic layer plane growth [31]. Depending upon variables such as the number of crystallites, their initial size, relative orientation, amount of interspersed non-ordered material, maximum elevated temperature and cooling rate, varying amounts of internal structure will result [23].

The TEM micrographs suggest that LII measurements should only be made below the vaporization threshold where the soot still resembles its initial structure in terms of primary particle size and aggregate morphology. However, accurate f_v measurements have been performed using fluences well above the vaporization threshold [26]. Therefore, it is pertinent to examine the effects of these varying morphological changes upon the LII signal over a wide range of fluences. The two-pulse experiments described below provide insight into these effects.

2.3 Two-laser pulse experiments

Having identified the changes induced in the soot at various excitation laser fluences, questions remain as to the timescale on which they occur and the effect of these changes upon the LII signal. We have designed three types of double-pulse LII experiments to address these issues.

2.3.1 Dual-pump experiment. The first set of experiments, which will be referred to as the dual-pump experiment, investigates the effect of the morphological changes in the soot upon the LII signal. In these experiments, the pulse energies of the two beams were varied synchronously while being maintained equal. The time separation between the two laser pulses was set at 10 μs, a value sufficient to allow the soot heated by the first laser pulse to cool to the local flame temperature [16–20]. The LII signal produced by the second laser pulse measures the effect of the changes in the soot upon the resulting incandescence. Since various energies induce different changes in the soot, the effects on the optical signal can be measured. To scale the very different incandescence magnitudes produced with the different laser energies, the integrated signal from the second pulse (hereafter referred to as LII(2)) was divided by the integrated LII signal produced by a single isolated laser pulse. Prompt detection gates of 50 and 100 ns were used to obtain the integrated signals.

Figure 7 plots the ratio of LII(2)/LII(reference) versus the fluence of the two laser pulses. Except for very low laser fluences, a significant decrease in LII(2) occurs as a result of the structural changes/mass loss induced by pulse one. The TEM images show little graphitization and no noticeable mass loss for very low laser fluences as illustrated in Fig. 5a. The enhanced LII(2) at very low fluences is consistent with modest thermal annealing induced by the first laser pulse that enhances the absorption and emission properties of the soot. The annealing may produce a more ordered solid-state structure as reactive radical sites and carbon atom layer-plane defects are removed.

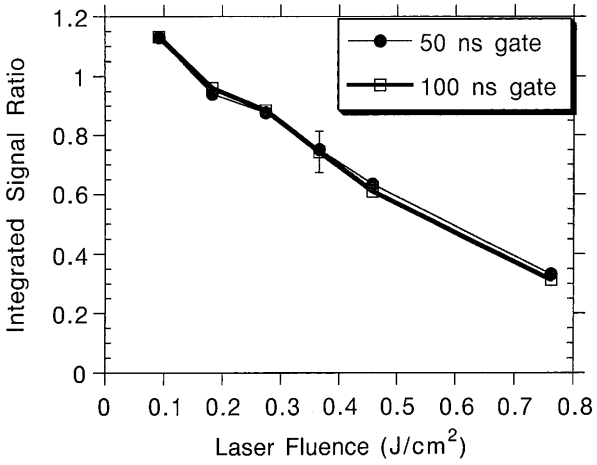

Fig. 7. Ratio of LII(2) to LII in the absence of a prior laser pulse as a function of pulse one fluence. In these pump-pump experiments, the fluence of both pulses one and two were equal

These results are relevant to LII experiments that employ a high repetition rate laser or which examine very low velocity flows. In either case, a second laser pulse could heat soot that had been heated by a prior laser pulse thus altering the observed LII signal.

2.3.2 Pump-probe experiment. The dual-pump experiments, while quantifying the effect of morphological changes upon LII(2) for a given set of experimental conditions, do include the effects induced by both laser pulses. Hence this set of measurements does not provide an isolated measure of the changes induced solely by pulse one. In fact, it could be argued that the morphological changes produced by the first laser pulse do not affect the LII signal at all but merely render the soot highly sensitive to a second laser pulse which is actually responsible for the structural changes that alter LII(2). Therefore, we designed a second series of experiments that employ a weak nonperturbative probe as pulse two to minimize its effect on the soot. In these experiments, the time delay between the two laser pulses was maintained at 10 μs, as in the dual-pump experiment. The fluence of pulse one is likewise varied over a range of values, but the fluence of pulse two is maintained at the smallest practical value in an effort to minimize any effects it could have upon the soot. Similar to the prior measurements, LII(2) was ratioed to the LII signal produced by a single isolated laser pulse (equivalent to the probe pulse fluence). Similar detection gates were used as in the dual-pump experiments.

Figure 8 shows this ratio as a function of pulse one laser fluence. Similar to the experiments with equal pulse energies, the induced morphological changes result in a decrease in the absorption and emission properties of the soot except at very low laser fluences for pulse one. The similarity of these results using a very low energy probe to those using equal energies for pulses one and two suggests that the decreases in the soot absorption and emission properties result from

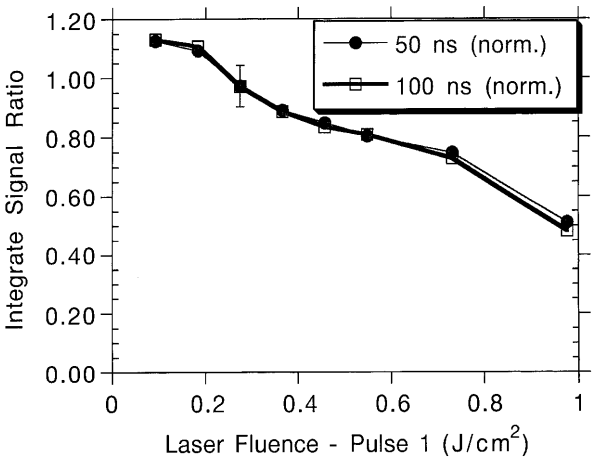

Fig. 8. Ratio of LII(2) to LII in the absence of a prior laser pulse as a function of pulse one fluence. In these pump/probe experiments, the fluence of pulse two was maintained at a low value as the fluence of pulse one was varied

pulse one, independently of pulse two. With the exception of mild graphitization (see Fig. 5a), extensive graphitization induced by pulse one results in a decrease in the LII signal. Thus on a timescale of 10 μs, the soot structural/physical properties and corresponding radiative characteristics are irrevocably changed in the LII process

2.3.3 Constant temperature experiment. Having quantified the effect of the structural/morphological changes induced in the soot through analysis of the second LII signal, a question still remains as to the fluence levels at which mass loss occurs. Previous work has identified a vaporization threshold occuring roughly at 0.5 J/cm^2 at 1064 nm based on pulsed laser transmission measurements, consistent with measurements performed in [16] at 532 nm. The TEM micrograph shown in Fig. 5d, clearly shows that surface mass loss and/or fragmentation occurs at laser fluences above this value. The hollow particles in the TEM images of Figs. 5b,c suggest that interior mass loss and structural/morphological changes are induced at fluences below this value. The results of the dual-pump and pump-probe experiments reveal a decreased integrated signal for laser fluences beyond 0.2 J/cm^2, consistent with this speculation.

Perhaps a more important question is what mass loss mechanisms occur at different laser fluences. Theory predicts that mass loss through surface vaporization occurs at high fluences during the excitation laser pulse. The changes observed in Figs. 5b,c, however, are consistent with an alternative mass loss mechanism consisting of volatilization/vaporization of interior material, unaccounted for by theory. If these changes involve mass loss, then less incandescent material will remain. If these changes occur on a timescale at which the particle is still at an elevated temperature, a faster signal temporal decay rate will result.

Changes in the absorption/emission properties can also explain the lower LII intensity in the two-pulse experiments discussed thus far. In the previous two-pulse experiments comparing LII signals produced by laser pulses of equal intensity, altered absorption/emission properties could explain the lower LII intensity produced by the second laser pulse. However, given that radiative energy loss is a minor contribution for particle temperatures below 3500 K [18], changes in the optical properties of the soot as a result of the graphitization will not dominate the temporal evolution of the signal. Instead, such changes will alter the peak particle temperature for a given excitation laser fluence. Thus only mass loss will appreciably affect the temporal decay rate of the LII signal.

2.4 Mass loss

One approach to test for this alternative mass loss mechanism would use a weak, nonperturbative probe laser pulse scanned in time relative to the first laser pulse. Changes in the intensity and/or temporal decay of LII(2) would then signal when such changes occur or at least when such changes become significant enough to affect the incandescence. The difficulty lies in the convolution of LII(1) with LII(2). For times after the first laser pulse at which the soot is still at elevated temperatures, the signal produced by the probe adds in a nonlinear manner to the remaining LII(1). This is to be expected given that radiative intensity scales as T^4 as described by the Stefan-Boltzman law. Hence the signal during and after the probe pulse cannot be deconvolved into contributions from pulse one and pulse two. Thus we sought an alternative approach to circumvent these difficulties.

The approach adopted compares two different pathways that heat the soot to the same temperature. First, the LII signal from a single laser pulse with a fluence of 0.3 J/cm^2 (well below the vaporization threshold) is collected. This signal serves as the reference. Second, a two-pulse experiment is performed in which the fluence of pulse one is systematically varied while the fluence of pulse two is adjusted to produce the same peak amplitude for LII(2) as the reference pulse. There are a range of fluences for pulse one and two that can accomplish this. The rationale for this approach is that the intensity of the signal at any wavelength will be indicative of the temperature of the object for short wavelengths well beyond the peak emission intensity. (This assumes constant soot volume fraction within the same measurement location within the flame.) Therefore, if no mass loss occurred in the soot as a result of pulse one, then the temporal decay of the signal produced by pulse two should be identical to that of the signal produced by the reference pulse. In this case, the soot behaves similarly regardless of the path that brought it to the peak temperature corresponding to the LII peak reference intensity. Because the intensity of laser pulse two is adjusted to give the same signal as that of the reference, this will mask any intensity changes due to structural/morphological changes. If mass loss occurs, (assuming the same initial temperature) the temporal decay rate of the signal will be different from that of the reference pulse.

Figure 9 shows the observed time-resolved LII signals for a laser pulse separation of 100 ns. For energies of pulse one lower than the vaporization threshold (Figs. 9a,b) no discernable change produced by pulse one preheating appears in the temporal evolution of the signal after pulse two. Thus the graphitization process and formation of hollow shell structures do not produce significant mass loss or a substantially different particle heat capacity. For fluences of pulse one above 0.45 J/cm^2 (Fig. 9c), a marked change in the temporal decay is evident. This change likely reflects mass loss

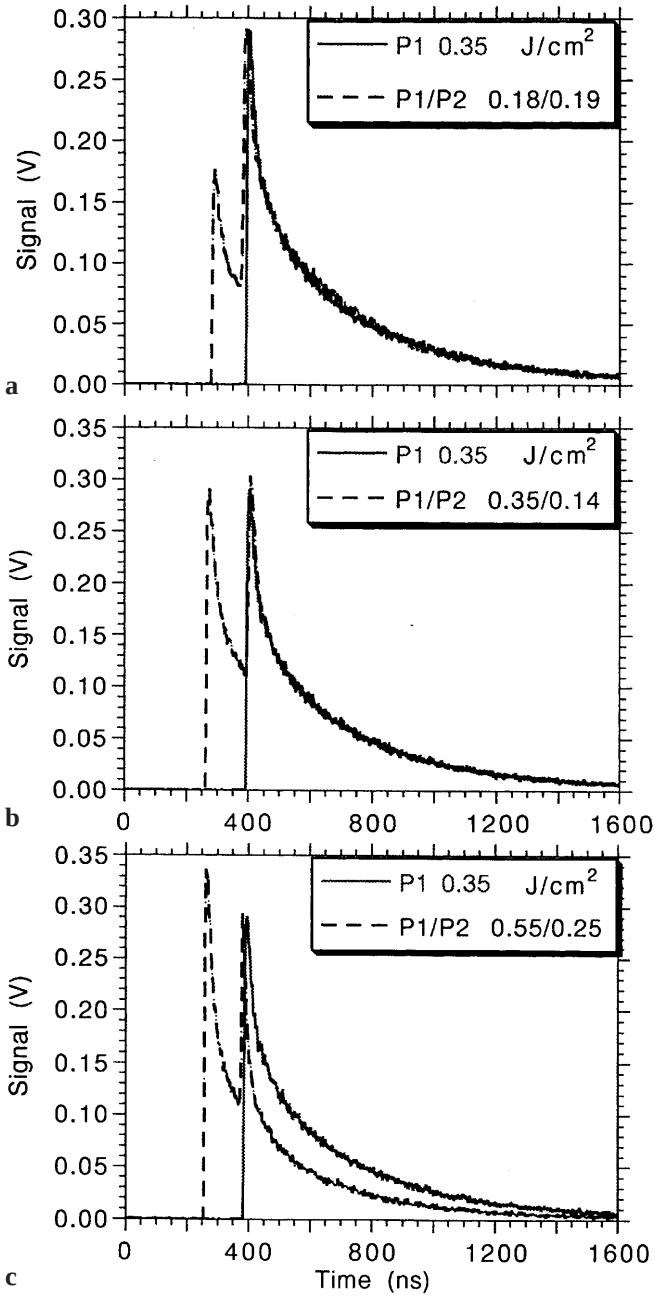

Fig. 9a–c. Illustration of the temporally resolved LII signals produced by the two laser pulses with 100 ns separation compared with the LII signal produced by the reference pulse. See text for details

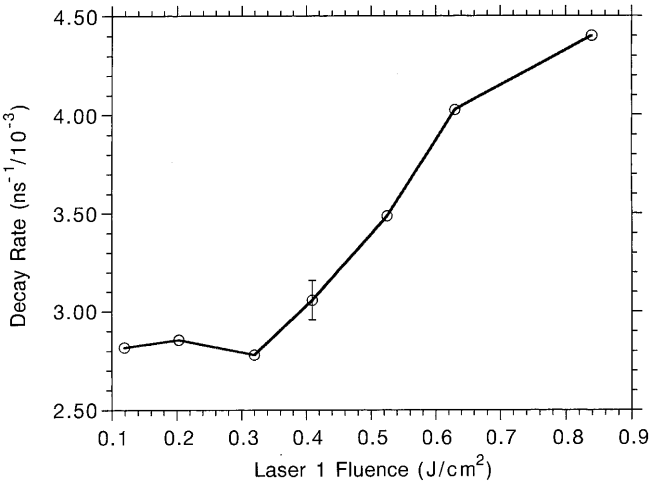

Fig. 10. LII signal decay rate measured after the second laser pulse as a function of the fluence in laser pulse one in the constant temperature experiments. The indicated decay rate is the slower decay rate found by fitting the temporal decay of the LII signal to a double exponential function

due to vaporization, thus leaving less material to incandesce. As Fig. 9 shows, the structural/morphological changes produced at low laser fluences ($< 0.45\,J/cm^2$) by a single laser pulse do not appear to affect the LII signal on a timescale relevant to a volume fraction measurement using one laser pulse. This is more clearly shown in Fig. 10. No change in the slow decay rate is observed in the LII signal produced by pulse two for fluences of pulse one below the apparent vaporization threshold of $0.45\,J/cm^2$. As previously stated, evidence that mass loss occurs at all laser fluence lies in the TEM micrographs (Fig. 5) which show that morphological changes occur at all laser fluences and in the previously discussed two-pulse results which show that these changes also affect the absorption and emission properties of LII(2) (as shown by Figs. 8 and 9). Because the temporal evolution of the signal (LII2) in these constant-temperature experiments remains unaltered for fluences of pulse one below the vaporization threshold of $0.45\,J/cm^2$ at 1064 nm as shown in Fig. 10, we conclude that only mass rearrangement and not mass loss occurs.

Similar experiments were also conducted at time separations of 250, 500, and 1000 ns between the two pulses in an effort to discern the time at which morphological changes affect the LII signal for laser fluences below the vaporization threshold. At time separations of 500 ns or greater, the slow decay rate of LII(2) becomes larger than that of a single pulse of equal energy for fluences of pulse one below $0.45\,J/cm^2$, in constrast to the results obtained with a time separation of 100 ns. This likely reflects the higher fluence of pulse two required to obtain the same amplitude as the reference pulse.

Further measurements are in progress. These observations also indicate that primary particle size determinations will not be affected if they are carried out at fluences below the vaporization threshold using the initial (first 500 ns) portion of the observed LII signal decay. This is because in the absence of a change in the temporal decay rate of the signal, significant mass loss apparently does not occur. In this case the signal still reflects the amount of the original material, albeit now in a graphitized form.

3 Conclusions

The dependence of the LII intensity upon laser fluence is detection specific. The plateau region previously observed reflects the trade-off between increased peak intensity and a faster decay with increased laser fluence. Therefore, it does not reflect a constant elevated temperature of the soot. TEM micrographs reveal that physical changes occur in the laser-heated soot for all laser fluences of practical use in LII measurements. With increasing fluence, increased graphitization occurs up to the vaporization threshold of approximately

$0.45 \pm 0.05\,\mathrm{J/cm^2}$ at 1064 nm. Beyond this value, interior and exterior mass loss occurs through vaporization.

Double-pulse experiments reveal that these graphitization changes are induced by one laser pulse and for fluences above $0.1\,\mathrm{J/cm^2}$ at 1064 nm. This change is manifested by initially higher and then lower LII signal intensities for the second pulse as its fluence is varied, indicative of altered emission/absorption properties of the partially graphitized soot and different cooling rates when significant mass loss occurs. Double-pulse experiments with a short time delay between the excitation laser pulses of 100 ns reveal that these structural changes do not involve significant mass losses for fluences below an observed vaporization fluence threshold. For fluences above this vaporization threshold, changes leading to a lower LII signal (lower peak intensity and faster temporal decay) occur during the excitation laser pulse. While LII has yielded accurate relative f_v measurements at laser fluences above and below the vaporization threshold, use of fluences below $0.45\,\mathrm{J/cm^2}$ appears not to alter the soot sufficiently to impact the signal within practical signal collection times after the excitation laser pulse.

Unlike f_v measurements, primary particle size determinations by LII are more sensitive to changes in soot morphology because the analysis uses the majority of the temporal evolution of the signal. The dual-pump and pump/probe results suggest that even though graphitization and hollow shells ensue at fluences below $0.45\,\mathrm{J/cm^2}$, these structural/ morphological changes do not involve mass loss but merely a change in the absorption and emission properties. Therefore these effects will likely not affect the determination of primary particle size through LII provided that fluences below the vaporization threshold are used.

Acknowledgements. This work was supported through NASA contract NAS3-27186 with Nyma Inc. Professor Ticich and Mr. Brock Stephens gratefully acknowledge support through the Ohio Aerospace Institute ASEE summer faculty fellowship and accompanying student program.

References

1. R.L. Vander Wal, K.J. Weiland: Appl. Phys. B **59**, 445 (1994)
2. B. Quay, T.W. Lee, T. Ni, R.J. Santoro: Combust. Flame **97**, 394 (1994)
3. N.A. Tait, D.A. Greenhalgh: Ber. Bunsen-Ges. Phys. Chem. **97**, 1619 (1993)
4. F. Cignoli, S. Benecchi, G. Zizak: Appl. Opt. **33**, 5778 (1994)
5. T. Ni, J.A. Pinson, S. Gupta, R.J. Santoro: Appl. Opt. **34**, 7083 (1995)
6. C.R. Shaddix, K.C. Smyth: Combust. Flame **107**, 418 (1996)
7. C.R. Shaddix, J.E. Harrington, K.C. Smyth: Combust. Flame **99**, 723 (1994)
8. C.R. Shaddix, K.C. Smyth: Combust. Flame **107**, 418 (1996)
9. R.L. Vander Wal: Twenty-Sixth Symposium (International) on Combustion (The Combustion Institute, Pittsburgh, PA 1996) p. 2269
10. R.L. Vander Wal: Combust. Sci. Technol. **118**, 343 (1996)
11. R.L. Vander Wal: Appl. Opt. **35**, 6548 (1996)
12. R.L. Vander Wal, Z. Zhou, M.Y. Choi: Combust. Flame **105**, 462 (1996)
13. R.L. Vander Wal: Exp. Fluids **23**, 281 (1997)
14. J. Appel, B. Jungfleisch, M. Marquardt, R. Suntz, H. Bockhorn: Twenty-Sixth Symposium (International) on Combustion (The Combustion Institute, Pittsburg, PA 1996) p. 2387
15. R.L. Vander Wal, D.L. Dietrich: Appl. Opt. **34**, 1103 (1995)
16. L.A. Melton: Appl. Opt. **23**, 2201 (1984)
17. C.J. Dasch: Appl. Opt. **23**, 2209 (1984)
18. D.L. Hofeldt: SAE Tech. Pap. 930079 (Society of Automotive Engineers, Warrendale, PA 1993)
19. B. Mewes, J.M. Seitzman: Appl. Opt. **36**, 709 (1997)
20. S. Will, S. Schraml, A. Leipertz: Twenty-Sixth Symposium (International) on Combustion (The Combustion Institute, Pittsburgh, PA 1996) p. 2277
21. R.L. Vander Wal, T.M. Ticich, A.B. Stephens: Combust. Flame, in press (1998)
22. R.L. Vander Wal, M.Y. Choi, K.-O. Lee: Combust. Flame **102**, 200 (1995)
23. F.A. Heckman: J. Rubber Chem. Technol. **37**, 1245 (1967)
24. H.R. Leider, O.H. Krikorian, D.A. Young: Carbon **11**, 555 (1973)
25. P.-E. Bengtsson, M.J. Alden: J. Appl. Phys. B **60**, 51 (1995)
26. R.L. Vander Wal, K.A. Jensen: Appl. Opt. **37**, 1607 (1998)
27. R.J. Santoro, T.T. Yeh, J.J. Horvath, H.G. Semerjian: Combust. Sci. Technol. **53**, 89 (1987)
28. F.G. Emmerich: Carbon **33**, 1709 (1995)
29. H.B. Palmer, C.F. Cullis: In: *The Chemistry and Physics of Carbon*, Vol. I, ed. by P.L. Walker (Marcel Dekker, New York 1965) p. 265
30. R.D. Heidenreich, W.M. Hess, L.L. Ban: J. Appl. Cryst. **1**, 1 (1968)
31. D. Ugarte: Chem. Phys. Lett. **207**, 474 (1993)